Modeling GPR Signal for Fast and Accurate Characterization of Layered Media

Subrata Maiti
Department of ECE
NIT, Rourkela
Odisha-769008, India
Email: smaiti@nitrkl.ac.in

Sarat Kumar Patra
Department of ECE
NIT, Rourkela
Odisha-769008, India
Email: skpatra@nitrkl.ac.in

Amitabha Bhattacharya
Department of E&ECE
IIT Kharagpur
West Bengal-721302, India
amitabha@ece.iitkgp.ernet.in

***Abstract*—Accuracy and efficiency are two important objectives of modeling ground penetrating radar (GPR) signal. Achieving both together is a driving factor for advanced research in the state of art for GPR community. Full wave model (FWM) promises great accuracy to detect layered media. However time efficiency of FWM is poor compared to other simplified models. This work presents a new plane wave model (PWM) based on simplified expression of an FWM. The proposed model is capable of detecting layered media in far field condition with great accuracy and efficiency. Based on this scheme a monostatic frequency domain GPR system is realized in laboratory environment. The model is validated by testing water layer and comparing accuracy and efficiency with an existing FWM scheme.**

***Keywords*—Ground penetrating radar (GPR), Green's function, inverse modeling, SFCW radar, layered media**

I. INTRODUCTION

The accuracy and efficiency of ground penetrating radar (GPR) detection largely depend on the signal modeling scheme. Compared to the numerical models [1–3] analytical models [4–13] are more efficient for a problem specific solution. Among analytical modeling schemes common midpoint (CMP) [4], [5], common reflection methods [6–8], layer stripping (LS) [9–11] are some of the popular approaches for fast characterization of layered media. These schemes are based on plane wave assumption and extracted data posseses limited accuracy when dispersion is significant in the media. In this respect full wave models (FWM) [12], [13] are more accurate techniques to retrieve complete electro-magnetic (EM) properties of layered media. In the field of monostatic stepped frequency continuous wave (SFCW) GPR in far field configuration Lambot *et al.* have contributed significantly by proposing an FWM [12] which has been successfully applied for water content estimation [14]. The time required to compute this FWM is still significantly high making it unsuitable for real time applications.

In this work first an FWM is derived based on electric field equivalent magnetic current density at antenna phase center. The common reflection method is modified by a spreading factor based on the simplified formula of the proposed FWM to yield a plane wave model (PWM) which is simultaneously fast and accurate. A comprehensive analysis on the both types of models and GPR detection results on water layer with an assembled monostatic SFCW GPR system in laboratory strongly support the superiority of proposed PWM.

II. MODELING GPR SIGNAL

A. GPR Transceiver System Model and its Assumptions

The SFCW radar setup presented in Fig. 1(a) is assembled with a Vector Network Analyzer (VNA, E5071C of Agilent), TEM horn antenna (BBHA 9120A, Schwarzbeck Mess-Elektronik) and a wooden tank (138.5 cm $\times$ 98.5 cm $\times$ 30 cm) containing material under test. A metal plate (122 cm $\times$ 81 cm) is kept at the bottom of the tank to control the boundary condition. For monostatic configuration and far field measurement,

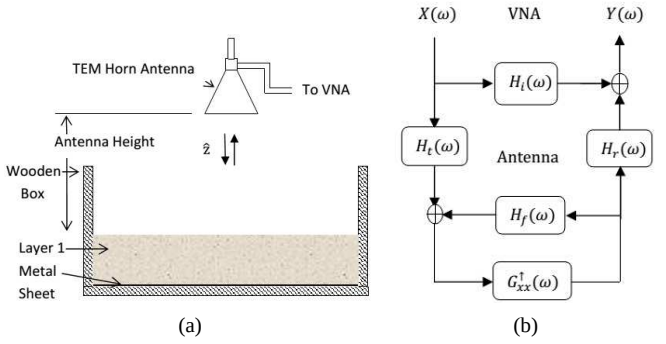

(a) (b)

Fig. 1. (a) Laboratory experimental setup for the GPR system. (b) Block diagram representing the VNA-antenna-multilayered medium system [12].

the antenna can be assumed as a point source and receiver. The signal is assumed to be propagating in normal direction only i.e in z directions. The VNA, antenna and sub-surface are modelled as linear systems in series and parallel as shown in Fig. 1(b). Therefore the VNA measured complex reflection coefficient $S_{11}(\omega)$ is expressed as following.

$$S_{11}(\omega) = \frac{Y(\omega)}{X(\omega)} = H_i(\omega) + \frac{H_t(\omega)\, G^{\uparrow}_{xx}(\omega) H_r(\omega)}{1 - H_f(\omega)\, G^{\uparrow}_{xx}(\omega)} \quad (1)$$

where $X(\omega)$ is the transmitted signal and $Y(\omega)$ is the received signal at the VNA-Antenna connector reference plane; $H_i(\omega)$ is the return loss of the antenna, $H_t(\omega)$ is the transmit transfer function of the antenna, $H_r(\omega)$ is the receive transfer function of the antenna, and $H_f(\omega)$ represents the feedback loss transfer function. $G^{\uparrow}_{xx}(\omega)$ is the Green's function representing the air-subsurface media. All these frequency dependent linear transfer functions (LTF) can be evaluated by a set of measurements with known targets like large size perfect electric conductor (PEC) placed at several distances from antenna and then solving a set of linear equations [15].

B. FWM Green's Function

The air-ground surface media is modeled as a 3D multi-layered media consists of N horizontal layers separated by N-1 interfaces as illustrated in the Fig. 2. Any single n^{th} layer

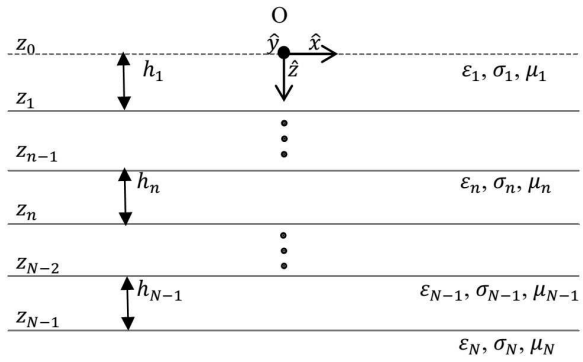

Fig. 2. Model configuration of N-layered medium with a point source.

is homogeneous and is characterized by its EM parameters electric permittivity (ϵ_n), electric conductivity (σ_n), magnetic permeability (μ_n) and its thickness (h_n). The permeability μ_n is assumed to be free space value μ_0. The antenna assumed to be point source and receiver at its phase center is located at the origin O of the coordinate system. Let us assume that the transmitted electric field is E^t_{xp} directing only towards x-direction at the antenna phase center. By applying Huygen's field equivalence principle as explained in [16] ($pp.\ 575-581$), the equivalent magnetic current density $\mathbf{M}_s$ can be expressed by following relation.

$$\mathbf{M}^s = -2\hat{\mathbf{n}} \times \hat{\mathbf{x}} E^t_{xp} = -2E^t_{xp}\hat{\mathbf{y}} \tag{2}$$

And equivalent electric current density

$$\mathbf{J_s} = \mathbf{0} \tag{3}$$

Here $\hat{\mathbf{n}}$ is normal to the antenna face and is in z-direction i.e. the direction of EM wave propagation. Now antenna can be replaced by the imaginary (equivalent) magnetic current source $\mathbf{M}_s$ at the antenna phase center. The radiated far field due to this magnetic source can be derived by solving Maxwell's equations in 3-dimensions. The methods for evaluating scattered EM fields by solving Maxwell's equation for EM wave propagation in the multilayered media are discussed in various literatures [17–19]. The Green's function $G^{\uparrow}_{xx}(\omega)$ is defined here as the backscattered x-directed electric field for a unit-strength x-directed transmitted electric field at the antenna phase center at frequency ω rad/s.

The spatial domain Green's function at the source point $((x, y, z) = 0)$ is expressed as

$$G^{\uparrow}_{xx}(0,\omega) = \frac{1}{4\pi}\int_0^{+\infty} \tilde{G}^{\uparrow}_{xx}(k_\rho,\omega)\, k_\rho dk_\rho \tag{4}$$

The integration variable k_ρ is a spectral domain parameter. The analytical expression of the spectral domain Green's function is derived (derivation not mentioned) and its final form is given below.

$$\tilde{G}^{\uparrow}_{xx}(k_\rho,\omega) = \left[R^{TE}_n - R^{TM}_n\right] e^{-2\Gamma_n h_n} \tag{5}$$

where R^{TM}_n is the transverse magnetic global reflection coefficient and R^{TE}_n is the transverse electric global reflection coefficient accounting for all reflections from the multilayered interfaces as explained in [17] ($pp.\ 48-53$). Γ_n is the vertical wave number of the n^{th} defined as $\Gamma_n = \sqrt{k_\rho^2 - k_n^2}$, where k_n is free space propagation constant of n^{th} defined by the relations $k_n^2 = -\zeta_n\eta_n$, $\zeta_n = i\omega\mu_n$, and $\eta_n = \sigma_n + i\omega\epsilon_n$. In order to do fast integration the integration path should avoid the integrand singularities and the function oscillation should be minimized. It is observed that by applying constant phase path of integration as explained in [20], the integration becomes fast reducing the computation time significantly.

The spectral domain Green's function for monostatic configuration derived by [12] by assuming TEM horn antenna as an infinitesimal horizontal x-directed dipole is given below.

$$\tilde{G}^{\uparrow}_{xx}(k_\rho,\omega) = \left[R^{TM}_n\frac{\Gamma_n}{\eta_n} - R^{TE}_n\frac{\zeta_n}{\Gamma_n}\right] e^{-2\Gamma_n h_n} \tag{6}$$

The Green's function expression in (5) is similar to the Green's function expression in (6). Let us denote the FWM mentioned in [12] as FWM-1 and the proposed one as FWM-2.

C. Simplification of FWM to derive PWM

In this section the FWM-2 Green's function presented in the Section II-B is simplified and important findings are used to modify the common reflection method. Let us consider the case of single layer media and reflection by an infinite size PEC. From (4) and (5) the expression of Green's function is written as following.

$$G^{\uparrow}_{xx}(\omega) = \frac{1}{4\pi}\int_0^{+\infty}\left[R^{TE}_1 - R^{TM}_1\right] e^{-2\Gamma_1 h_1} k_\rho dk_\rho \tag{7}$$

For reflection by PEC, ${R_1}^{TE} = -1$, ${R_1}^{TM} = 1$, and $\Gamma_1 = \sqrt{k_\rho^2 - k_1^2}$. k_1 can be expressed as following.

$$k_1 = \sqrt{-\zeta_1\eta_1} = \sqrt{-i\omega\mu_1(\sigma_1 + i\omega\epsilon_1)} = \beta_1 - i\alpha_1 = -i\gamma_1 \tag{8}$$

Here β_1 is the phase constant and α_1 is the attenuation constant and $\gamma_1\,(= ik_1)$ is complex propagation constant in another form. Therefore (8) is simplified as

$$G^{\uparrow}_{xx}(\omega) = \frac{-1}{2\pi}\int_0^{+\infty} e^{-2h_1\sqrt{{k_\rho}^2 + {\gamma_1}^2}} k_\rho dk_\rho \tag{9}$$

Now applying integration by parts $G^{\uparrow}_{xx}(\omega)$ in (9) is simplified to the following relation.

$$G^{\uparrow}_{xx}(\omega) = \frac{1}{2\pi}\left[-\frac{\gamma_1 e^{-2h_1\gamma_1}}{2h_1} - \frac{e^{-2h_1\gamma_1}}{(2h_1)^2}\right] \tag{10}$$

In above expression second term is attenuated by distance square and it can be neglected for far field calculation. Therefore Green's function is further simplified as given below.

$$G^{\uparrow}_{xx}(\omega) = \frac{-1}{2\pi}\frac{e^{-2h_1\gamma_1}}{(2h_1/\gamma_1)} \tag{11}$$

$\frac{1}{2\pi(2h_1/\gamma_1)}$ in (11) is the spreading factor for the signal.

Now the common reflection method is modified according to the simplified expression of FWM-2 in (11) to make it very accurate without compromising its efficiency. For plane wave propagation in layered media, the contribution of first order reflection $\left(\hat{r}^1_{n,n+1}\right)$ from n^{th} interface (z_n) to the overall Green's function is given by the following relation [8].

$$\left(\hat{r}^1_{n,n+1}\right) = r_{n.n+1}\prod_{j=1}^{n-1}\left(1-\left(r_{j,j+1}\right)^2\right)\prod_{j=1}^{n} exp(-2\gamma_j h_j) \tag{12}$$

where γ_j is the j^{th} layer complex propagation parameter, $r_{j,j+1}$ is reflection coefficient at z_j layer interface given by

$$r_{j,j+1} = \frac{Z_{j+1}-Z_j}{Z_{j+1}+Z_j}. \tag{13}$$

Z_j is the impedance of j^{th} layer media given by $Z_j = \sqrt{\frac{\zeta_j}{\eta_j}}$. Now plane wave assumption is true when source is in infinite distance from the target. For finite distance case we like to modify this relation (12) with spreading factor according to the expression of FWM-2 in (11) as given below.

$$R^1_{n,n+1} = \left(\frac{1}{2\pi i\sum_{j=1}^{n} 2h_j/\gamma_j}\right)\left(\hat{r}^1_{n,n+1}\right) \tag{14}$$

Where $R^1_{n,n+1}$ is the contribution of 1^{st} order reflection from interface z_n to the Green's function. The superscript of $R^1_{n,n+1}$ denotes the order of reflection coefficient. It can be observed in (14) that one complex term $'i'$ is introduced at the denominator of the expression. This is required to have phase matching between (12) and (14). With h^2 variation is significant the (14) is modified as following.

$$R^1_{n,n+1} = \left(\frac{\hat{r}^1_{n,n+1}}{2\pi i}\right)\left(\frac{1}{\sum_{j=1}^{n} 2h_j/\gamma_j} + \frac{1}{\left(\sum_{j=1}^{n} 2h_j\right)^2}\right) \tag{15}$$

Therefore overall Green's function contributed by reflections from all the layer interfaces z_1 to z_{N-1} with maximum order N_o can be expressed as following.

$$G^{\uparrow PWM}_{xx}(\omega) = \sum_{i=1}^{N_o}\sum_{k=1}^{N-1} R^i{}_{k,k+1} \tag{16}$$

Let us denote this Green's function obtained by plane wave approximation as plane wave Green's function $G^{\uparrow PWM}_{xx}$ and the model as plane wave model (PWM). Also define the $G^{\uparrow PWM}_{xx}$ obtained by considering only h variation term from (16) as PWM-1 and the $G^{\uparrow PWM}_{xx}$ obtained by considering both h and h^2 variation terms as PWM-2. It can be observed that no integration is required to compute the Green's function $G^{\uparrow PWM}_{xx}$ compared to the FWMs. This makes computation of PWM very efficient.

III. COMPARISON OF MODELS AND THEIR INVERSION

A. Comparison of GPR Signal Models

A rigorous analysis has been carried out for PWMs and FWMs in terms of complex Green's functions values across frequencies in large parameter vector space and efficiency of their computations. In all respect we have found that performances of both FWM-1 [12] and FWM-2 are same. PWM-1 and PWM-2 are closely matching with FWMs in terms of accuracy while promising tremendous speed of computation. Here a brief analysis on comparison of all the models in terms of frequency averaged %RMS difference and computation efficiency is presented.

It is observed that frequency response of FWM-1 differs with FWM-2 with a constant K and phase shift 180^o. In order to compare FWMs, FWM-1 is divided by $-$K. Again from (11) and (14) it is observed that PWMs and FWMs Green's functions have got 90^o phase shift. To make proper comparison among all the models, both the FWMs are multiplied by $-1i$. Important point to note here is that these phase and amplitude changes by a constant have no impact on GPR inversion as extracted G_{xx} by calibration process and modeled G_{xx} both have same constant multiplied. A single layer media is considered with wide range of parameter vector space $(2 < \epsilon_r < 101; 10 < \sigma < 10^4 mS/m; 1 < h < 10^3 cm)$. To sweep such a wide range of parameters, they are varied exponentially. Total 4851 (11 along ϵ_r, 21 along σ and 21 along h) iterations are completed to compute all types of Green's functions. Any two models (1 and 2) are compared by frequency averaged %RMS difference between their Green's functions ($G^{\uparrow 1}_{xx}$ and $G^{\uparrow 2}_{xx}$) by following formula.

$$\%RMS\_Diff. = 100\times\sqrt{\frac{\sum_{i=1}^{N_f}\left|\left(G^{\uparrow 1}_{xx}(\omega_i)\right)-\left(G^{\uparrow 2}_{xx}(\omega_i)\right)\right|^2}{\sum_{i=1}^{N_f}\left|\left(G^{\uparrow 2}_{xx}(\omega_i)\right)\right|^2}} \tag{17}$$

The N_f is the number of frequency points in the total frequency band. With frequency separation of 40 MHz, total 101 N_f are considered in the frequency band 0.5 to 4.5 GHz. The order of reflection (N_o) for PWMs is varied from 5 to 25 with observation that N_o higher than 20 has got no effect on G_{xx} value in the mentioned parameter vector space. The summary of analysis is presented in Table I. The worst case %RMS difference for three different ϵ_r values i.e. 2, 16 and 81 over whole range of $(\sigma - h)$ plane are considered for presentation. For PWMs N_o value of 5 and 20 are presented. It is observed that the worst case %RMS differences among FWM2, FWM1 and PWM2 are very small over the wide parameter vector space and the worst case value for this simulation is found to be 0.74542 %. The efficiency of each model as time required to compute single Green's functions over 101 N_f for a single layer media is presented in last row of Table I. Each model was run at least 1000 times in an 1.93 GHz core i3 laptop to calculate the average computation time.

TABLE I. COMPARISON OF MODELS.

Worst case frequency averaged %RMS difference with FWM-2					
ϵ_r	FWM-1	PWM-1		PWM-2	
		$N_o = 5$	$N_o = 20$	$N_o = 5$	$N_o = 20$
2	0.7454	4.3716	4.3737	0.0957	0.0957
16	0.4531	6.0280	2.6236	5.5612	0.4994
81	0.3598	21.1715	2.5402	21.0441	0.6873
Processing time in milliseconds					
	2280.0	6.2414	6.9968	6.1191	7.3611

Based on this analysis it can be concluded that the complex frequency response of proposed PWM matches well with the FWMs as we consider for the higher order reflections and h^2

variation term. The stability and noise performance of PWMs and FWM-2 are expected to be same as FWM-1 due to small %RMS difference among the Green's functions.

B. Model Inversion

For inversion of model, objective function $\Phi(b)$ is defined in least square sense as following.

$$\Phi(b) = \left|G_{xx}^{\uparrow *}(\omega) - G_{xx}^{\uparrow}(\omega, b)\right|^T \left|G_{xx}^{\uparrow *}(\omega) - G_{xx}^{\uparrow}(\omega, b)\right| \tag{18}$$

where $G_{xx}^{\uparrow *}(\omega)$ is the vector containing measured and $G_{xx}^{\uparrow}(\omega, b)$ is the vector containing simulated Green's function of the multilayered media. The parameters vector b (consists of $\mu_n, \epsilon_n, \sigma_n, h_n$) needs to be estimated by minimizing the objective function $\Phi(b)$ in Eq. (18). A gradient based approach i.e. Neadler-Mead algorithm of Matlab is implemented to minimize $\Phi(b)$. Since gradient based technique can't converege unless the starting parameters values are in global basin, a layer stripping (LS) technique (details not given) is utilized to get preliminary information of layer thickness and electrical parameters of media. In fact with application of accurate modeling scheme i.e. PWM, LS is giving promising results for the laboratory testing case presented in result section.

IV. RESULTS AND DISCUSSION

At first GPR calibration was carried out following the procedure mentioned in [15] so that all the frequency dependent LTFs are evaluated across the frequency band. The whole testing setup (shown in Fig. 1(a)) was kept at roof top without control of temperature and shielding from external RF interferences. The frequency range 800 MHz to 4000 MHz was swept with frequency step of 4 MHz. Due to manual adjustment of the antenna stand, our height measurement inaccuracy was around +/-2 mm. From analysis mentioned in [15] it is understood that mm inaccuracy of antenna height measurement during calibration process causes significant error for estimating LTFs and leads to detection error. Accordingly the frequency range of 800 MHz to 2000 MHz was selected for achieving least %RMS error between measured and modeled Green's function by inversion.

Water is a homogenous media and its frequency dependent electrical parameters are well defined by various research works [21–23]. The complex dielectric constant (ϵ_e) of water is a function of EM wave frequency (f), temperature (T) and salinity (S). The characteristics of ϵ_e is accurately described by the Klein-Swift model [21] below 10 GHz microwave frequency. The salinity (S) of drinking water is negligible. The real part of ϵ_e is the relative dielectric constant ϵ_r and is denoted by static relative permittivity ϵ_s as given by (19). The imaginary part of ϵ_e contributes the frequency dependent conductivity $\sigma(f)$ as given by (20).

$$\epsilon_s(T) = 88.045 - 0.4147T + 6.295\times10^{-4}T^2 + 1.075\times10^{-5}T^3 \tag{19}$$

$$\sigma(f) = \sigma_s + \frac{\epsilon_s - \epsilon_\infty}{1 + \left(\frac{f}{f_r}\right)^2}\left(\frac{f}{f_r}\right) 2\pi f \epsilon_0 \tag{20}$$

Where ϵ_∞ is the permittivity at infinite frequency with value as 4.9, σ_s is static ionic conductivity of water, f_r is the relaxation frequency of water as given in (21) [23].

$$f_r(T) = 2\pi/(1.1109\times10^{-10} - 3.824\times10^{-12}T + 6.938\times10^{-14}T^2 - 5.096\times10^{-16}T^3) \tag{21}$$

GPR measurement was conducted to collect the S_{11} data while keeping the antenna above a water layer. The water layer thickness was measured by ruler as approximately 3.6 cm. The metal plate was kept at the bottom of the water layer to control the boundary condition. The atmosphere temperature was reported as 29-30 degree centigrade during afternoon at the time of experiment. Water temperature measured by a thermometer had shown 39 degree centigrade during experiment as water layer was exposed to sunlight. With unavailability of standard conductivity meter in our laboratory, static conductivity (σ_{s2}) was taken as an optimization parameter for GPR inversion. Relative dielectric constant ϵ_{s2} and conductivity ($\sigma_2(f)$) were calculated by model i.e. (19) and (20) respectively. Total three parameters i.e. antenna height (h_1), water layer thickness (h_2), and its static conductivity (σ_{s2}) were optimized by GPR inversion using FWMs and PWMs. For both the PWMs maximum up to 20^{th} order reflection was considered to calculate the Green's function. To find the initial parameter values LS technique was utilized. Total 31 frequency points were considered in 1200 MHz bandwidth for model inversion to achieve better efficiency without compromising the detection accuracy.

The results of inversion are presented in the TABLE II. It is observed that the proposed PWMs are as accurate as FWMs to detect the water layer parameters. Interesting point to observe here is that the PWM-1 which is most approximated model of FWM-2, yielded lower %RMS error compared to other three models and it took more time for detection compared to the PWM-2. It is quite possible that a less accurate model matches better with the measurement data when GPR measurement is affected by calibration error, noise and interferences. In general the timing efficiency achieved by PWMs is enormous compared to FWMs. Fig. 3 presents plot of the measured and the modeled Green's function for the water layer in frequency and time domain. It shows good agreement of phase characteristics and partial agreement of amplitude characteristics between the measured and the modeled Green's functions for all the models.

TABLE II. WATER PARAMETERS ESTIMATED BY PWMS AND FWMS.

Model used	Estimated Parameters				
	h_1 (cm)	h_2 (cm)	σ_{s2} (mS/m)	Processing time (s)	%RMS Error
LS	32.1645	3.7573	336.1152	0.8803	–
PWM-1	32.2464	3.6171	337.8612	0.4590	13.4317
PWM-2	32.1792	3.6184	339.8806	0.4043	13.9080
FWM-1	32.1789	3.6173	340.3352	132.1153	13.9166
FWM-2	32.1793	3.6172	340.3069	131.6505	13.9079

V. CONCLUSION

In this work an SFCW monostatic GPR system based on fast and accurate modeling schemes (PWMs) is proposed. Laboratory experiments with water layer proved that PWMs are capable of estimating layered media's parameters with accuracy comparable with FWMs and their speed of computation is enormous. The gradient based approach is capable of inverting the models for single layer media with aid of layer

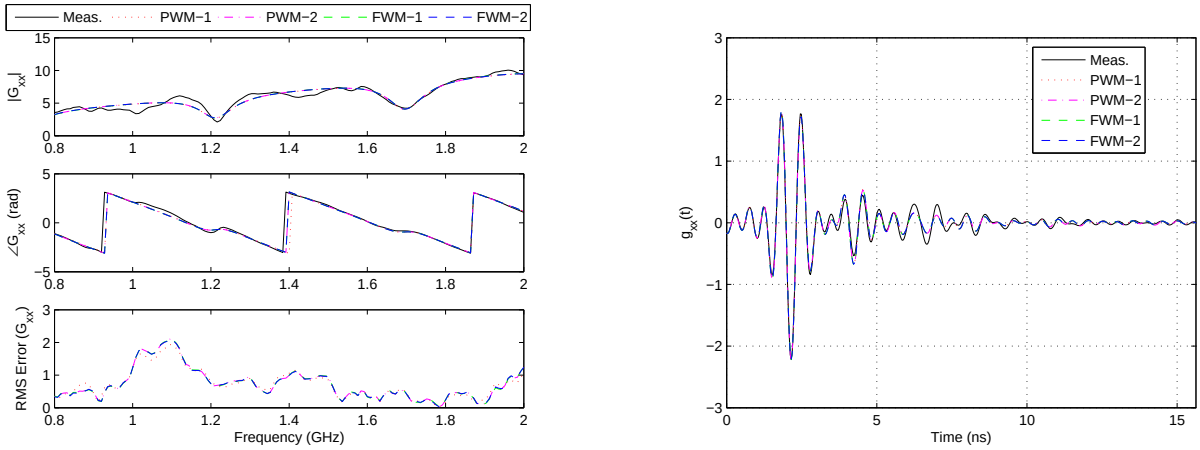

(a) (b)

Fig. 3. Measured and modeled Green's function for the water layer represented in (a) Frequency and (b) Time domain.

stripping technique. Clearly the proposed integrated approach is suitable for real time applications. Though the PWMs are very fast to detect the layered media, the GPR calibration process to extract the linear transfer functions makes the scheme inefficient and GPR detection complexity high. The future work should focus on to simplify the process of calibration and develop a robust global optimization scheme which would be capable of inverting the model with large number of parameters efficiently.

REFERENCES

[1] K. Belli, C. M. Rappaport, H. Zhan, and S. Wadia-Fascetti, "Effectiveness of 2-d and 2.5-d fdtd ground-penetrating radar modeling for bridge-deck deterioration evaluated by 3-d fdtd," *Geoscience and Remote Sensing, IEEE Transactions on*, vol. 47, no. 11, pp. 3656–3663, 2009.

[2] C. Warren and A. Giannopoulos, "Creating finite-difference time-domain models of commercial ground-penetrating radar antennas using taguchis optimization method," *Geophysics*, vol. 76, no. 2, pp. G37–G47, 2011.

[3] T. M. Millington and N. J. Cassidy, "Optimising gpr modelling: A practical, multi-threaded approach to 3d fdtd numerical modelling," *Computers & Geosciences*, vol. 36, no. 9, pp. 1135–1144, 2010.

[4] S. Tillard and J.-C. Dubois, "Analysis of gpr data: wave propagation velocity determination," *Journal of Applied Geophysics*, vol. 33, no. 1, pp. 77–91, 1995.

[5] P. Protiva, J. Mrkvica, and J. Machác, "Estimation of wall parameters from time-delay-only through-wall radar measurements," *Antennas and Propagation, IEEE Transactions on*, vol. 59, no. 11, pp. 4268–4278, 2011.

[6] G. Serbin and D. Or, "Ground-penetrating radar measurement of soil water content dynamics using a suspended horn antenna," *Geoscience and Remote Sensing, IEEE Transactions on*, vol. 42, no. 8, pp. 1695–1705, 2004.

[7] H. Liu, X. Xie, and M. Sato, "Accurate thickness estimation of a backfill grouting layer behind shield tunnel lining by cmp measurement using gpr," in *Ground Penetrating Radar (GPR), 2012 14th International Conference on*. IEEE, 2012, pp. 137–142.

[8] Z.-l. Huang and J. Zhang, "Determination of Parameters of Subsurface Layers Using GPR Spectral Inversion Method," vol. 52, no. 12, pp. 7527–7533, 2014.

[9] U. Spagnolini, "Permittivity measurements of multilayered media with monostatic pulse radar," *Geoscience and Remote Sensing, IEEE Transactions on*, vol. 35, no. 2, pp. 454–463, 1997.

[10] A. Loizos and C. Plati, "Accuracy of ground penetrating radar horn-antenna technique for sensing pavement subsurface," *Sensors Journal, IEEE*, vol. 7, no. 5, pp. 842–850, 2007.

[11] S. Caorsi and M. Stasolla, "A layer stripping approach for em reconstruction of stratified media," *Geoscience and Remote Sensing, IEEE Transactions on*, vol. 52, no. 9, pp. 5855–5869, 2014.

[12] S. Lambot, E. C. Slob, I. van den Bosch, B. Stockbroeckx, and M. Vanclooster, "Modeling of ground-penetrating radar for accurate characterization of subsurface electric properties," *Geoscience and Remote Sensing, IEEE Transactions on*, vol. 42, no. 11, pp. 2555–2568, 2004.

[13] A. Kalogeropoulos, J. Van Der Kruk, J. Hugenschmidt, J. Bikowski, and E. Brühwiler, "Full-waveform gpr inversion to assess chloride gradients in concrete," *Ndt & E International*, vol. 57, pp. 74–84, 2013.

[14] F. Jonard, L. Weihermller, K. Z. Jadoon, M. Schwank, H. Vereecken, and S. Lambot, "Mapping field-scale soil moisture with l-band radiometer and ground-penetrating radar over bare soil," *IEEE Transactions on Geoscience and Remote Sensing*, vol. 49, no. 8, pp. 2863–2875, 2011.

[15] M. R. M. Ardekani and S. Lambot, "Full-wave calibration of time- and frequency-domain ground-penetrating radar in far-field conditions," *Geoscience and Remote Sensing, IEEE Transactions on*, vol. 52, no. 1, pp. 664–678, 2014.

[16] C. A. Balanis, *Antenna theory: analysis and design*. John Wiley & Sons, 2001.

[17] W. C. Chew, *Waves and fields in inhomogeneous media*. IEEE press New York, 1995.

[18] G. Dural and M. I. Aksun, "Closed-form green's functions for general sources and stratified media," *Microwave Theory and Techniques, IEEE Transactions on*, vol. 43, no. 7, pp. 1545–1552, 1995.

[19] S. Lambot *et al.*, "Hydrogeophysical characterization of soil using ground penetrating radar," Ph.D. dissertation, Ph. D. thesis, Catholic Univ. of Louvain, Louvain-la-Neuve, Belgium, 2003.

[20] S. Lambot, E. Slob, and H. Vereecken, "Fast evaluation of zero-offset green's function for layered media with application to ground-penetrating radar," *Geophysical Research Letters*, vol. 34, no. 21, 2007.

[21] L. Klein and C. T. Swift, "An improved model for the dielectric constant of sea water at microwave frequencies," *Antennas and Propagation, IEEE Transactions on*, vol. 25, no. 1, pp. 104–111, 1977.

[22] P. J. W. Debye, *Polar molecules*. Chemical Catalog Company, Incorporated, 1929.

[23] A. Stogryn, "Equations for calculating the dielectric constant of saline water (correspondence)," *IEEE transactions on microwave theory and Techniques*, pp. 733–736, 1971.